

# WASP-180Ab: Doppler tomography of an hot Jupiter orbiting the primary star in a visual binary

L.Y. Temple,<sup>1\*</sup> C. Hellier<sup>1</sup>, D.R. Anderson<sup>1</sup>, K. Barkaoui<sup>7,2</sup>, F. Bouchy<sup>3</sup>, D.J.A. Brown<sup>4,5</sup>, A. Burdanov<sup>7</sup>, A. Collier Cameron<sup>6</sup>, L. Delrez<sup>8</sup>, E. Ducrot<sup>7</sup>, D. Evans<sup>1</sup>, M. Gillon<sup>7</sup>, E. Jehin<sup>7</sup>, M. Lendl<sup>3</sup>, P.F.L. Maxted<sup>1</sup>, J. McCormac<sup>4</sup>, C. Murray<sup>8</sup>, L. D. Nielsen<sup>3</sup>, F. Pepe<sup>3</sup>, D. Pollacco<sup>4,5</sup>, D. Queloz<sup>8</sup>, D. Ségransan<sup>3</sup>, B. Smalley<sup>1</sup>, S. Thompson<sup>8</sup>, A.H.M.J. Triaud<sup>9</sup>, O.D. Turner<sup>3,1</sup>, S. Udry<sup>3</sup>, R.G. West<sup>4</sup>, B. Zouhair<sup>2</sup>

<sup>1</sup>*Astrophysics Group, Keele University, Staffordshire, ST5 5BG, UK*

<sup>2</sup>*Oukaïmeden Observatory, High Energy Physics and Astrophysics Laboratory, Cadi Ayyad University, Marrakech, Morocco*

<sup>3</sup>*Observatoire astronomique de l'Université de Genève 51 ch. des Maillettes, 1290 Sauverny, Switzerland*

<sup>4</sup>*Department of Physics, University of Warwick, Gibbet Hill Road, Coventry, CV4 7AL, UK*

<sup>5</sup>*Centre for Exoplanets and Habitability, University of Warwick, Gibbet Hill Road, Coventry CV4 7AL, UK*

<sup>6</sup>*SUPA, School of Physics and Astronomy, University of St. Andrews, North Haugh, Fife, KY16 9SS, UK*

<sup>7</sup>*Space sciences, Technologies and Astrophysics Research (STAR) Institute, Université de Liège, Allée du 6 Août 17, 4000 Liège, Belgium*

<sup>8</sup>*Cavendish Laboratory, J J Thomson Avenue, Cambridge, CB3 0HE, UK*

<sup>9</sup>*School of Physics & Astronomy, University of Birmingham, Edgbaston, Birmingham, B15 2TT, UK*

Accepted XXX. Received YYY; in original form ZZZ

## ABSTRACT

We report the discovery and parametrisation of WASP-180Ab, a hot Jupiter confirmed by the detection of its Doppler shadow and by measuring its mass using radial velocities. We find the  $0.8 \pm 0.1 M_{\text{Jup}}$ ,  $1.29 \pm 0.07 R_{\text{Jup}}$  planet to be in a misaligned, retrograde orbit around an F7 star with  $T_{\text{eff}} = 6500 \text{ K}$  and a moderate rotation speed of  $v \sin i_{\star} = 21 \text{ km s}^{-1}$ . The host star is the primary of a  $V = 10.7$  binary, where a secondary separated by  $5''$  contributes  $\sim 30\%$  of the light. WASP-180Ab therefore adds to a small sample of transiting hot Jupiters known in binary systems. A 4.6-day modulation seen in the WASP data is likely to be the rotational modulation of the companion star, WASP-180B.

**Key words:** techniques: spectroscopic – techniques: photometric – planetary systems – stars: rotation

## 1 INTRODUCTION

In the age of high resolution spectrographs, the possibilities for detailed characterisation of exoplanets are expanding. We are able to map the motion of a hot Jupiter across the disc of its host star as it transits, via a method called Doppler tomography. This method consists of the direct detection of distortions to stellar line profiles that occur due to the occultation of the star by a smaller orbiting body (e.g. Collier Cameron et al. 2010; Siverd et al. 2018; Temple et al. 2018a). In mapping the motion of this distortion as a function of phase, it is possible to determine the current projected spin-orbit misalignment angle,  $\lambda$ , which gives insight

to the dynamical history of the system. Doppler tomography is especially suited to hotter targets which elude radial velocity characterisation due to a lack of spectral lines. It can also reveal the effects of internal stellar motions on the surface of a star, such as differential rotation and convection (Cegla et al. 2016b) and stellar pulsations (see, e.g. Temple et al. 2017).

In this work we present a newly discovered hot Jupiter, WASP-180Ab, transiting the primary star of a visual binary in a misaligned, retrograde orbit.

This discovery is in line with theories surrounding Lidov-Kozai oscillations being responsible for the high obliquities seen in some hot-Jupiter systems (e.g. Anderson et al. 2016; Storch et al. 2017). It has long been theorized that a distant stellar companion can induce such oscillations in

\* E-mail: l.y.temple@keele.ac.uk

**Table 1.** Details of the photometric and spectroscopic observations of WASP-180Ab carried out for this work.

Telescope/Instrument	Date	Notes
WASP-North	2009–2011	8329 points
WASP-South	2011–2012	4359 points
TRAPPIST-South	2018 Jan 5	z'. 10s exp.
TRAPPIST-North	2018 Jan 12	z'. 11s exp.
SPECULOOS-Callisto	2018 Jan 22	z'. 8s exp.
ESO 3.6-m/HARPS	2018 Jan 5	21 spectra through transit
Euler/CORALIE	2015–2018	9 RVs
ESO 3.6-m/HARPS	2018 Mar	6 RVs

a Jupiter’s orbit, leading to high-eccentricity migration of the planet which produces a misaligned, short-period orbit. This would then be followed by realignment of the host star with the planet’s orbit via tidal dissipation, an effect that would be less efficient for stellar hosts lacking convective envelopes, and thus this theory is consistent with the observed tendency of systems with stars hotter than  $\sim 6250$  K being more likely to have planetary orbits which are misaligned with respect to the stellar rotation axis (Winn et al. 2010; Albrecht et al. 2012).

Besides WASP-180Ab there are 11 known transiting hot Jupiters and one transiting hot Saturn in binary systems, listed in the NASA exoplanet archive (Akeson et al. 2013). The number of such planets is low compared to the total number of known exoplanet systems, which may be partially the result of selection bias. Since the light from a planet host in a binary system is often diluted in the light of the other star, the apparent transit depth is reduced, making detection via the transit method more difficult.

## 2 DATA AND OBSERVATIONS

WASP-180 is a known binary, listed as WDS 08136-0159 in the Washington Double Star Catalogue (Mason et al. 2001), with the two stars having *Gaia* magnitudes of 10.9 and 11.8. *Gaia* DR2 confirms the two stars to have the same parallax and proper motions, and we calculate the angular separation to be  $4.854''$  (Gaia Collaboration et al. 2016, 2018). This separation is sufficient to avoid contamination in high-resolution spectroscopic observations of the system.

We observed WASP-180A from November 2009 to March 2012 using the SuperWASP-North telescope (Polacco et al. 2006) located at the Roque de los Muchachos Observatory in La Palma, as well as the WASP-South telescope (Hellier et al. 2011) located at the South African Astronomical Observatory (SAAO).

Upon detecting a 3.4-d transit-like signal in the WASP data we obtained focused photometry with TRAPPIST-South (Jehin et al. 2011), resolving the two stars. These data were sufficient to show that the transit is of the brighter of the two stars, WASP-180A, but were otherwise of low quality and so we exclude the lightcurve from further analysis.

We proceeded to obtain radial velocity (RV) measurements with the Euler/CORALIE (Queloz et al. 2001) spectrograph. WASP-180A is a fast rotating F star with broad lines giving large RV errors, so the CORALIE RVs ruled

**Table 2.** RV measurements for WASP-180A taken using the CORALIE and HARPS spectrographs for this work. The values in italics are of low signal-to-noise due to an auto-guiding issue during observation.

BJD <sub>TDB</sub>	RV (km s <sup>-1</sup> )	$\sigma_{RV}$ (km s <sup>-1</sup> )	BS (km s <sup>-1</sup> )	$\sigma_{BS}$ (km s <sup>-1</sup> )
-2,450,000				
CORALIE:				
7092.644031	28.96	0.05	-0.18	0.10
7697.849714	28.96	0.06	0.01	0.12
7751.760876	29.02	0.06	-0.29	0.12
8077.824503	28.76	0.04	-0.12	0.08
8079.836204	28.90	0.05	-0.21	0.10
8094.796351	28.65	0.04	-0.00	0.08
8140.848419	28.90	0.06	-0.15	0.12
8212.592949	29.06	0.06	-0.11	0.12
8222.600891	28.95	0.07	-0.16	0.14
HARPS:				
8198.604103	29.02	0.02	-0.25	0.04
8199.643111	28.85	0.02	-0.04	0.04
8201.610172	29.01	0.02	-0.07	0.04
8202.589668	29.01	0.02	-0.06	0.04
8203.572959	28.87	0.02	-0.19	0.04
8204.571804	28.91	0.02	-0.01	0.04
HARPS (2018 Jan 05):				
8124.596974	28.99	0.02	-0.23	0.04
8124.607854	29.05	0.02	-0.21	0.04
8124.618421	28.98	0.02	-0.17	0.04
8124.629200	28.96	0.02	-0.15	0.04
8124.640806	28.90	0.02	-0.11	0.04
8124.650841	28.76	0.02	0.03	0.04
8124.661525	28.76	0.02	0.22	0.04
8124.672312	28.81	0.02	0.17	0.04
8124.683285	28.91	0.02	-0.12	0.04
8124.693748	29.02	0.02	-0.31	0.04
8124.704420	29.10	0.02	-0.48	0.04
8124.715299	29.20	0.03	-0.75	0.06
8124.725971	29.16	0.03	-0.63	0.06
<i>8124.736434</i>	<i>29.02</i>	<i>0.04</i>	<i>0.10</i>	<i>0.08</i>
<i>8124.746794</i>	<i>29.16</i>	<i>0.04</i>	<i>-0.03</i>	<i>0.08</i>
<i>8124.758090</i>	<i>28.35</i>	<i>0.05</i>	<i>-1.30</i>	<i>0.10</i>
8124.770313	28.91	0.02	-0.18	0.04
8124.780059	28.95	0.02	-0.22	0.04
8124.790510	28.91	0.02	-0.19	0.04
8124.801182	28.88	0.02	-0.22	0.04
8124.812062	28.91	0.03	-0.18	0.06

out a stellar-mass transit mimic, but were not sufficient to give a measurement of the planet’s mass. Thus we attempted Doppler tomography of a transit on the night of 2018 January 5 using the ESO 3.6-m/HARPS spectrograph (Pepe et al. 2002). Due to an auto-guiding issue three of the spectra obtained were of low signal-to-noise and were therefore discarded. Simultaneously during this transit we observed the lightcurve using TRAPPIST-South, using an aperture including both stars.

After tomographic confirmation of the planet we observed further follow-up lightcurves also using apertures including both stars. These were taken with TRAPPIST-North (Barkaoui et al. 2017, 2019) at the Oukaïmeden Observatory in Morocco and the SPECULOOS-Callisto telescope (Burdanov et al. 2018) at ESO Paranal Observatory. We also obtained 6 more RVs with HARPS to constrain the

planet’s mass. Details of the observations used in this work are provided in Table 1.

The RV measurements corresponding to each of the spectra obtained are listed in Table 2 with the corresponding bisector span (BS) measurements. These were measured from cross-correlation functions (CCFs) computed by cross-correlating the spectra using a mask matching a G2 spectral type, over a wide correlation window covering  $-320 \text{ km s}^{-1}$  to  $380 \text{ km s}^{-1}$ .

### 3 SPECTRAL ANALYSIS

We analysed a median-stacked HARPS spectrum created from the 18 HARPS spectra taken on the night of 2018 Jan 5, to obtain stellar parameters. We measured an effective temperature of  $6500 \pm 150 \text{ K}$  using the  $H\alpha$  line, while using the wings of the  $H\alpha$  profile to measure  $v \sin i_{\star} = 21 \pm 2 \text{ km s}^{-1}$ . We also used the Mg triplet feature to measure  $\log g_*$ , obtaining  $4.5 \pm 0.2$ , and measure the metallicity  $[\text{Fe}/\text{H}] = 0.09 \pm 0.19$ , assuming a microturbulence value of  $v_{\text{mic}} = 2 \text{ km s}^{-1}$ . Rather than extrapolate a value for the macroturbulence from the Doyle et al. (2014) calibration, which is valid only for stars up to  $6400 \text{ K}$ , we simply take the fitted  $v \sin i_{\star}$  to be an upper limit. We also used the MKCLASS program (Gray & Corbally 2014) to obtain a spectral type of F7 IV–V.

### 4 A DISTANT CO-MOVING COMPANION

The average parallax of WASP-180 measured by *Gaia* DR2 is  $3.885 \text{ mas}$  and the angular separation is  $4.854''$ , which indicates a binary separation of  $\sim 1400 \text{ AU}$ . This would imply an orbit of  $\sim 30000 \text{ yrs}$ , which is compatible with the fact that no significant change in separation or position angle is seen in measurements taken over a period of 120 years, as listed in the WDS.

Our photometry of WASP-180 was all extracted from an aperture including both A and B components. Thus we need to correct the lightcurves for dilution. We deduced correction factors in the different bands of SDSS  $z$  and Johnson  $V$ , the latter of which was used as an approximation for the WASP data. These are estimated from deducing the effective temperatures of the two stars from available photometry, as follows.

We fitted  $T_{\text{eff}}$ ,  $\log g_*$ , and  $[\text{Fe}/\text{H}]$  by comparing resolved catalogue photometry to the synthetic photometry of Casagrande & VandenBerg (2014, 2018) which uses the MARCS stellar models of Gustafsson et al. (2008). The stars were assumed to have identical  $[\text{Fe}/\text{H}]$ . Interstellar reddening was found to be poorly constrained by the photometry, and was instead fixed at  $E(B-V) = 0.01$ , derived from the 3D dust map of Green et al. (2014, 2015), adopting the closest reliable reddening measurements in the map, at approximately  $400 \text{ pc}$ . The choice of distance does not significantly affect the results, with the full line-of-sight reddening out to  $8 \text{ kpc}$  being  $E(B-V) = 0.02 \pm 0.02$ . Resolved photometry was found in PANSTARRS-1 (*grizy*), CMC15 (*r'*), DENIS (*JJK*), and 2MASS (*JHK*). The PANSTARRS-1 catalogue does not include uncertainties for the measurements, and

**Table 3.** Third light dilution factors and stellar flux ratios obtained for WASP-180.

Passband	Third Light	Flux Ratio
SDSS $z$	$0.325 \pm 0.007$	$0.48 \pm 0.01$
Johnson $V$	$0.260 \pm 0.006$	$0.351 \pm 0.008$

so a conservative uncertainty of  $0.1 \text{ mag}$  was assigned to all measurements in that catalogue.

Stellar parameters were derived by least-squares minimisation to find the minimum  $\chi^2$ , and uncertainties were determined by perturbing each parameter separately until a  $\delta\chi^2$  of 1 was reached. We found  $\log g_*$  to be poorly constrained by the photometry, with the entire range of the synthetic photometry grids ( $3.0 \leq \log g_* \leq 5.0$ ) failing to give  $\delta\chi^2 > 1$ . Temperatures of  $6540_{-30}^{+80} \text{ K}$  and  $5430_{-25}^{+30} \text{ K}$  were obtained for the A and B components respectively, as well as a joint  $[\text{Fe}/\text{H}]$  value of  $0.0_{-0.5}^{+0.1}$ . The fitting was also repeated four further times, excluding each of the four photometric catalogues (PANSTARRS-1, CMC15, DENIS, 2MASS) in turn. The mean and standard deviation of the parameters from these four additional fits are  $T_A = 6521 \pm 56 \text{ K}$ ,  $T_B = 5425 \pm 17 \text{ K}$ , and  $[\text{Fe}/\text{H}] = -0.01 \pm 0.01$ : in good agreement with the full fit, indicating that none of the four photometric surveys is significantly biased. The values of  $T_A$  we obtain are consistent with the value of  $T_{\text{eff}}$  from the spectral analysis (Sec. 3).

Using the stellar parameters from the full fit, and a fixed  $\log g_*$  of 4.5 (consistent with spectral analysis), flux ratios were estimated from the synthetic photometry for the  $z'$  and  $V$  bands. The fraction of light contributed by the secondary star was calculated, and thus the light curves corrected for the dilution of the planetary transit. The third light values and stellar flux ratios we obtained are given in Table 3.

### 5 COMBINED MCMC ANALYSIS

We use a Markov Chain Monte Carlo (MCMC) approach to fit the combined photometric and radial velocity data, as well as investigate the Rossiter–McLaughlin (RM) effect, which is the distortion of stellar line profiles caused by the occultation of a portion of the stellar surface by an orbiting body. We follow methods very similar to Temple et al. (2018b,a), whereby we conduct both an RM analysis and a tomographic analysis and adopt the better-constrained solution. The RM analysis involves detecting the line-profile distortions as an apparent overall shift in radial velocity measurements (e.g. Triaud 2017), whereas the tomographic analysis requires one to directly map the motion of the distortion caused by the occulting body across the line profiles as a function of phase (e.g. Brown et al. 2017; Temple et al. 2017).

The code we use is described by Collier Cameron et al. (2007); Pollacco et al. (2008); Collier Cameron et al. (2010). The combined photometric and RV fitting determines the orbital period  $P$ , the epoch of mid-transit  $T_C$ , the planet-to-star area ratio  $(R_p/R_{\star})^2$ , the transit duration  $T_{14}$ , the impact parameter  $b$ , the stellar reflex velocity semi-amplitude  $K_1$  and the barycentric system velocity  $\gamma$ . We use the value of  $T_{\text{eff}}$  obtained in the dilution correction as input, and interpolate

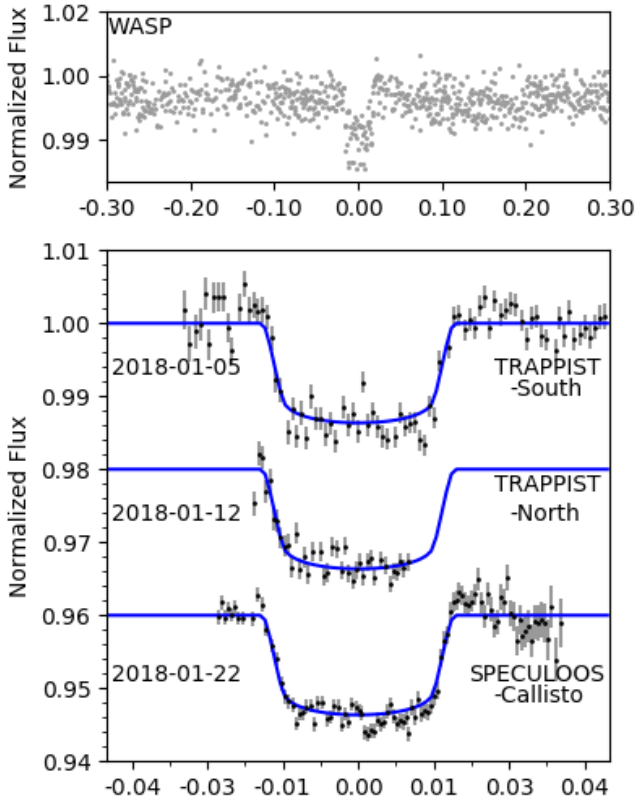
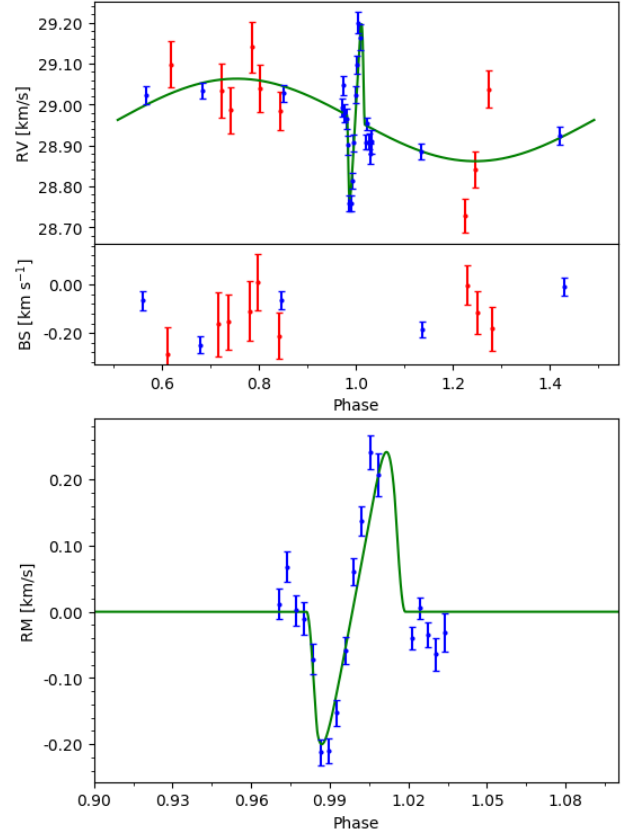


**Figure 1.** The WASP discovery photometry (top) and follow-up transit lightcurves (bottom) with the best-fitting model shown in blue. (see Section 5).

four-parameter limb darkening coefficients from the Claret (2000, 2004) tables in each step using the current value of  $T_{\text{eff}}$ . We calculate each value of the stellar mass  $M_{\star}$  using the Enoch–Torres relation (Enoch et al. 2010; Torres et al. 2010). In the fit we present we have assumed that the orbit is circular, as one would expect a hot Jupiter to circularise on a timescale shorter than its lifetime (Pont et al. 2011). However, a further fit was carried out to test this assumption, leading to an upper limit of  $e < 0.27$  (95% confidence). We display the photometry and best-fit transit model in Fig. 1.

The RM fit and Doppler tomography give values for  $v \sin i_{\star}$ ,  $\lambda$  and the system  $\gamma$ -velocity. We use the calibrations of Hirano et al. (2011) to fit the RM effect. For Doppler tomography, we assume a Gaussian profile for the perturbation to the stellar-line profiles and fit the intrinsic Full-Width at Half-Maximum (FWHM) of the perturbation,  $v_{\text{FWHM}}$ . Both methods also provide an additional constraint on the impact parameter  $b$ , although the tomographic method fits this quantity more directly. We estimate the start value for  $\gamma$  by fitting a Gaussian profile to the CCFs. We also apply the spectral  $v \sin i_{\star}$  as a prior in both fitting modes.

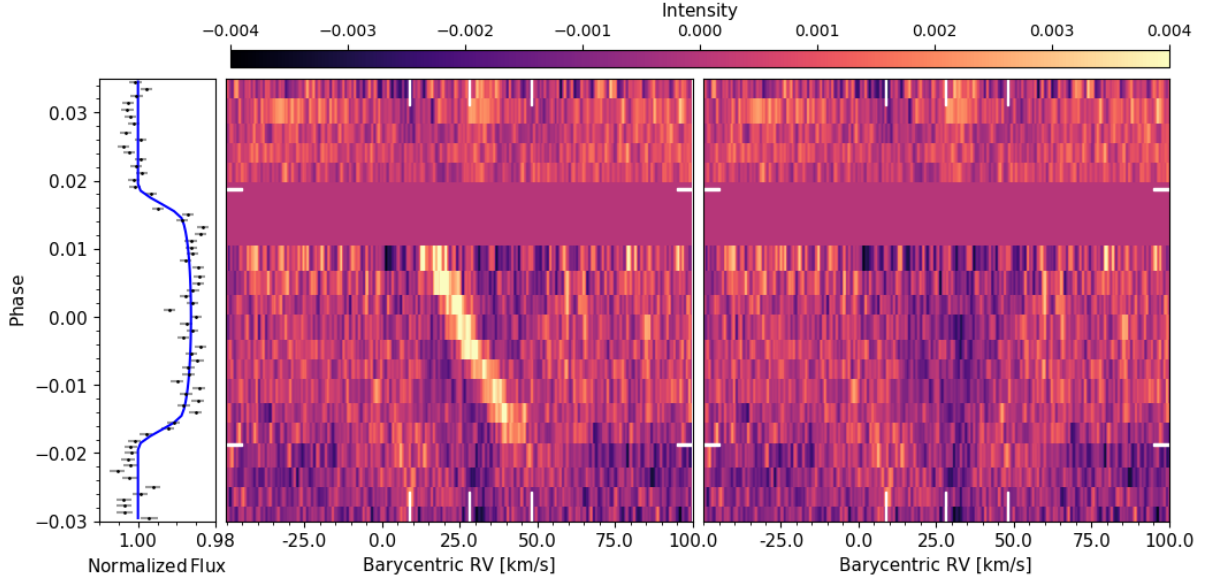
We find that the tomographic method was better able to constrain  $v \sin i_{\star}$  and  $\lambda$ . In the RM fit, the value of  $v \sin i_{\star}$  was less constrained, even when using the spectral  $v \sin i_{\star}$  as a prior. Thus we adopt the solution to the fit including Doppler tomography. We give the solutions for both methods in Table 4. The RV measurements used in this analysis and the best-fit RV and RM models are displayed in Fig. 2.



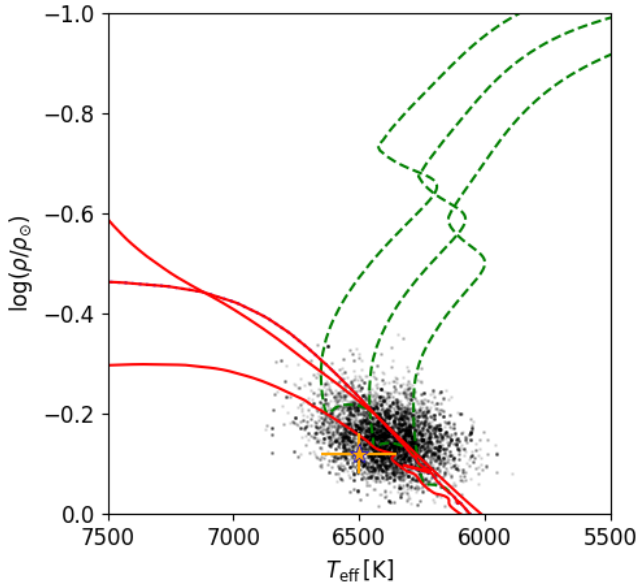
**Figure 2.** Top: All RV measurements of WASP-180A used in this work together with the best-fit model shown in green. The red points are CORALIE measurements and the blue points are HARPS measurements. Middle: the bisector (BS) measurements corresponding to the RVs in the top panel. Bottom: The RV measurements taken during transit and best-fit RM model.

Figure 3 shows the tomographic dataset used in this analysis. We have subtracted an average of the out-of-transit CCFs in the dataset from each CCF in order to display the residual bump due to the planet transit. The planet signal is strong and clear, moving in a retrograde direction. Due to excluding three of the CCFs (having low signal-to-noise) we are missing the transit egress. We also show the simultaneous photometric observation in Fig. 3 and a residuals plot produced by subtracting the planet model from the tomographic data.

Finally, we use the InfraRed Flux Method (IRFM Blackwell & Shallis 1977) to estimate the angular diameter of WASP-180A, and combine this with the *Gaia* DR2 parallax to estimate the radius of the planet host. We apply the correction to *Gaia* DR2 parallaxes suggested by Stassun & Torres (2018), obtaining a radius of  $1.09 \pm 0.06 R_{\odot}$ . This value is consistent with the result from our combined analysis.



**Figure 3.** The Doppler tomogram for WASP-180Ab, showing the strong retrograde planet trace (middle) and simultaneous photometric observation alongside (left). The right-hand panel shows the residuals remaining after subtracting the fit to the perturbation due to the planet (see Section 5). The white vertical dashes in the centre and right-hand panels mark the positions of  $\gamma$  and  $\gamma \pm v \sin i_*$  while the white horizontal dashes indicate the times of 1<sup>st</sup> and 4<sup>th</sup> contacts of the planet.



**Figure 4.** The best fitting evolutionary tracks and isochrones of WASP-180A obtained using BAGEMASS. Black points: individual steps in the MCMC. Dotted blue line: Zero-Age Main Sequence (ZAMS) at best-fit  $[\text{Fe}/\text{H}]$ . Green dashed lines: evolutionary track for the best-fit  $[\text{Fe}/\text{H}]$  and mass, plus  $1\sigma$  bounds. Red lines: isochrone for the best-fit  $[\text{Fe}/\text{H}]$  and age, plus  $1\sigma$  bounds. Orange star: measured values of  $T_{\text{eff}}$  and  $\rho_*$  for WASP-180A obtained in the spectral and photometric analyses respectively.

## 6 AGE DETERMINATION

We used the open source software BAGEMASS<sup>1</sup> to determine the age of the system following a Bayesian approach as

<sup>1</sup> <http://sourceforge.net/projects/bagemass>

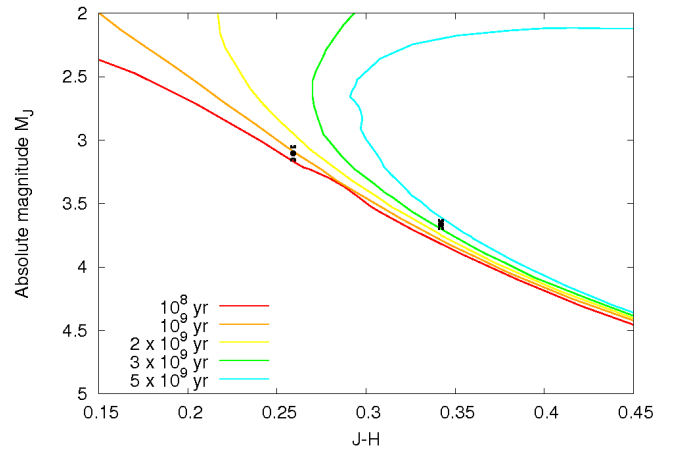


**Figure 5.** A colour-magnitude diagram showing the positions of WASP-180A and its comoving companion star with respect to isochrones from Marigo et al. (2017) for the ages 0.1, 1, 2, 3 and 5 Gyr ( $Z = 0.024 \sim [\text{Fe}/\text{H}] = 0.09$ ,  $Y = 0.27$ ).

described by Maxted et al. (2015). BAGEMASS takes constraints on the stellar temperature, density and metallicity to fit the age, mass and initial metallicity of a star using the GARSTEC stellar evolution code (Weiss & Schlattl 2008). We set  $T_{\text{eff}} = 6500 \pm 150$  K and  $[\text{Fe}/\text{H}] = 0.09 \pm 0.19$  (from spectral analysis) and  $\rho_*/\rho_{\odot} = 0.74 \pm 0.09$  (from photometry), and use different combinations of mixing lengths and He abundances. We find that the best-fitting parameter set was obtained when using a solar He abundance and mixing length, and thus adopt that solution. We give this solution in Table 4 while displaying the evolutionary tracks, isochrones and the distribution of explored values for this fit

**Table 4.** All system parameters obtained for WASP-180 in this work.

WASP-180: $V_T = 10.7$		
WASP-180A:		
1SWASP J081334.15–015857.9		
2MASS 08133416–0158579		
TIC ID:178367144		
RA = $08^{\text{h}}13^{\text{m}}34.15^{\text{s}}$ Dec = $-01^{\circ}58'57.9''$ (J2000)		
IRFM $T_{\text{eff}} = 7125 \pm 200$ K		
IRFM $\theta = 0.040 \pm 0.002$ mas		
	WASP-180A	WASP-180B
<i>Gaia</i> DR2 Proper Motions:		
RA	$-14.05 \pm 0.09$ mas	$-12.7 \pm 0.2$ mas
DEC	$-3.17 \pm 0.06$ mas	$-2.7 \pm 0.1$ mas
<i>Gaia</i> DR2		
Parallax:	$3.909 \pm 0.052$ mas	$3.862 \pm 0.073$ mas
$J$ (2MASS)	$10.11 \pm 0.05$	$10.68 \pm 0.03$
<i>Stellar parameters of WASP-180A from spectral analysis:</i>		
Parameter (Unit)	Value	
$T_{\text{eff}}$ (K)	$6500 \pm 150$	
$v \sin i_{\star}$ (km s $^{-1}$ )	$21 \pm 2$	
$\log g_{\star}$	$4.5 \pm 0.2$	
[Fe/H]	$0.09 \pm 0.19$	
$v_{\text{mic}}$	2 (assumed)	
Spectral type	F7 IV-V	
<i>Parameters from combined analyses:</i>		
Parameter (Unit)	DT Value (adopted):	RM Value:
$P$ (d)	$3.409265 \pm 0.000001$	$3.409265 \pm 0.000001$
$T_c$ (BJD <sub>TDB</sub> )	$2457763.3147 \pm 0.0003$	$2457763.3148 \pm 0.0003$
$T_{14}$ (d)	$0.130 \pm 0.001$	$0.1281 \pm 0.0009$
$T_{12} = T_{34}$ (d)	$0.015 \pm 0.001$	$0.0141 \pm 0.0007$
$R_p^2/R_{\star}^2$	$0.0124 \pm 0.0002$	$0.0125 \pm 0.0002$
$b$	$0.40 \pm 0.08$	$0.30 \pm 0.06$
$i$ ( $^{\circ}$ )	$87.4 \pm 0.6$	$88.1 \pm 0.5$
$a$ (AU)	$0.048 \pm 0.001$	$0.048 \pm 0.002$
$M_{\star}$ ( $M_{\odot}$ )	$1.3 \pm 0.1$	$1.3 \pm 0.1$
$R_{\star}$ ( $R_{\odot}$ )	$1.19 \pm 0.06$	$1.14 \pm 0.05$
$\log g_{\star}$ (cgs)	$4.39 \pm 0.03$	$4.43 \pm 0.02$
$\rho_{\star}$ ( $\rho_{\odot}$ )	$0.76 \pm 0.08$	$0.86 \pm 0.08$
$T_{\text{eff}}$ (K)	$6600 \pm 200$	$6600 \pm 100$
[Fe/H]	$0.1 \pm 0.2$	$0.1 \pm 0.2$
$M_p$ ( $M_{\text{Jup}}$ )	$0.8 \pm 0.1$	$0.9 \pm 0.1$
$R_p$ ( $R_{\text{Jup}}$ )	$1.29 \pm 0.07$	$1.24 \pm 0.06$
$\log g_p$ (cgs)	$3.06 \pm 0.07$	$3.11 \pm 0.06$
$\rho_p$ ( $\rho_J$ )	$0.38 \pm 0.07$	$0.46 \pm 0.07$
$K_1$ (km s $^{-1}$ )	$0.10 \pm 0.01$	$0.10 \pm 0.01$
$T_{p,A=0}$ (K)	$1570 \pm 50$	$1550 \pm 40$
$v \sin i_{\star}$ (km s $^{-1}$ )	$19.6 \pm 0.6$	$22 \pm 3$
$\lambda$ ( $^{\circ}$ )	$-162 \pm 5$	$-165 \pm 4$
$\gamma$ (km s $^{-1}$ )	$28.2 \pm 0.9$	$29.0 \pm 0.1$
$v_{\text{FWHM}}$ (km s $^{-1}$ )	$7.8 \pm 0.3$	–
<i>Parameters from BAGEMASS:</i>		
Parameter (Unit)	Value	
Age	$1.21 \pm 0.99$	
$M_{\star}$ ( $M_{\odot}$ )	$1.221 \pm 0.081$	
[Fe/H] <sub>init</sub>	$0.004 \pm 0.162$	

in Fig. 4. We find WASP-180A to be consistent with being on the main sequence, with an age of  $1.2 \pm 1.0$  Gyr.

We also extract stellar isochrones from Marigo et al. (2017) for stellar ages in the range  $10^8$ – $5 \times 10^9$  yr, using the metallicity from spectral analysis ([Fe/H]  $\sim 0.09$ ) to estimate appropriate mass fractions, obtaining  $Z = 0.024$  and  $Y = 0.27$ . These are displayed on a colour–magnitude diagram in Fig. 5 along with the positions of WASP-180A and WASP-180B. From the position of WASP-180B we can infer that the system has an age of  $\sim 1$  Gyr, and is likely to be non-evolved, which is consistent with our result from BAGEMASS.

## 7 ROTATIONAL MODULATION SEARCH

We perform a search of the WASP photometry following the method of Maxted et al. (2011), looking for rotational modulation or pulsation signals with frequencies of 0–1 cycles day $^{-1}$ . The data were split into three parts according to the observing season and camera used. We find a signal with an average amplitude of  $\sim 0.004$  mag and an average period of  $4.57 \pm 0.05$  days. The strongest peak in the first set of data lies at half the modulation period  $P_{\text{mod}}$ . The last set of data contained the clearest signal, and so was given double weight when computing the average. We display the periodograms for each set of data in Fig. 6, and give the individual best-fit amplitudes and periods in Table 5.

Using the measured  $v \sin i_{\star}$  from spectral analysis ( $21 \pm 2$  km s $^{-1}$ ) and the adopted stellar radius from the combined analysis ( $1.20 \pm 0.06 R_{\odot}$ ), we obtain an upper limit on the rotation period of WASP-180A, finding  $P_{\text{orb}} < 3.2$  days. This compares with the modulation period of  $\sim 4.6$  days, implying that the signal does not originate from rotational modulation in WASP-180A.

The co-moving companion star WASP-180B contributes  $\sim 30\%$  of the total flux, and so the true amplitude of the signal if originating from the secondary would be  $\sim 1\%$ , which is consistent with spot modulation on a fast-rotating later-type star. *Gaia* DR2 does not find any other close neighbours which may contribute to the total flux. Thus we believe the signal to belong to the visual companion star, which has a temperature of  $5430_{-25}^{+30}$  K. A rotation period of 4.6 days is fairly rapid for a star of  $T_{\text{eff}} = 5430_{-25}^{+30}$  K, which may imply a young age for the system, consistent with our BAGEMASS analysis in Section 6.

## 8 CONCLUSIONS AND DISCUSSION

WASP-180Ab is a  $0.8 \pm 0.1 M_{\text{Jup}}$ ,  $1.29 \pm 0.07 M_{\text{Jup}}$  hot Jupiter orbiting an F7 IV–V star with  $T_{\text{eff}} = 6500$  K and  $v \sin i_{\star} = 21$  km s $^{-1}$ . The planet’s large radius is in line with the expectation for a Jovian-mass planet in a close orbit around a fairly hot star to be inflated due to the high level of irradiation (e.g. Enoch et al. 2012; Sestovic et al. 2018).

The orbit is misaligned and retrograde, with a projected obliquity of  $\lambda = -162 \pm 5^{\circ}$ . This is also in line with known trends amongst hot Jupiters orbiting hot stars, since the majority of such planets are found to be in misaligned orbits (e.g. Winn et al. 2010; Albrecht et al. 2012; Dai & Winn 2017; Triaud 2017).

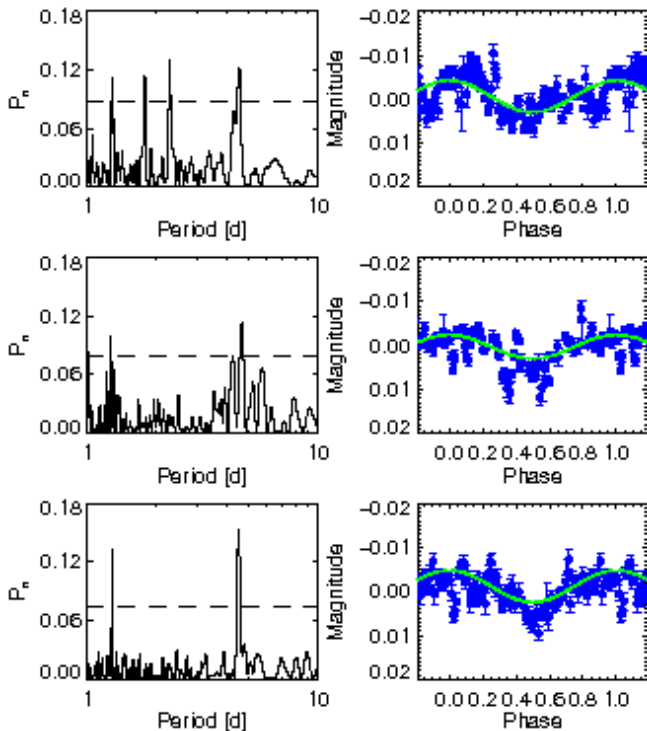


**Figure 6.** Results of the rotational modulation search of the WASP photometry of WASP-180A. The three rows show the periodogram (left) and phase-folded light curve (right) for each chunk of data, displayed in the same order as they are listed in Table 5. The horizontal dashed line in each of the periodograms corresponds to a confidence level of 99%.

WASP-180 is a known binary system. We can ask whether the secondary, WASP-180B, is responsible for the retrograde, misaligned orbit seen in WASP-180Ab, through having induced Lidov-Kozai oscillations leading to high-eccentricity migration of the planet. While this effect has long been thought able to produce such orbits, the pathways leading from high-eccentricity migration to the observed distribution of system obliquities are still a topic of avid research (e.g. Anderson et al. 2016; Storch et al. 2017). Anderson et al. (2016) places an upper limit on the final period of a hot Jupiter which has migrated due to Lidov-Kozai oscillations of  $P_{\text{orb}} < 4$  days, while Petrovich (2015) finds that the stellar separations of binaries with hot Jupiters are preferentially in the range 400–1500 AU, and so with  $P_{\text{orb}} = 3.4$  days and an estimated stellar separation of 1400 AU it is feasible for WASP-180Ab to have formed in this way.

There are 11 transiting hot Jupiters in binary systems listed in the NASA exoplanet archive (Akeson et al. 2013). With  $T_{\text{eff}} = 6500$  K and  $v \sin i_{\star} = 20 \pm 2$  km s $^{-1}$ , the planet host WASP-180A is also the second fastest rotating and second hottest host star of all planets in binary systems, including non-transiting planets, coming second to KELT-19Ab ( $T_{\text{eff}} = 7500$  K and  $v \sin i_{\star} = 84 \pm 2$  km s $^{-1}$  Siverd et al. 2018). Of the binary transiting planet systems currently known, only three have obliquity measurements: WASP-94Ab ( $T_{\text{eff}} = 6170$  K,  $\lambda = 151^{\circ}$  Neveu-VanMalle et al. 2014), WASP-85Ab ( $T_{\text{eff}} = 6112$  K,  $\lambda = 0^{\circ}$  Močnik et al. 2016) and

**Table 5.** The results of the rotational modulation search of the WASP photometry of WASP-180A. The strongest peak in the periodogram for the first set of data lies at  $P_{\text{mod}}/2$  (see Fig. 6).

Dates (HJD–2450000)	No. pts	Period (days)	Amplitude (mag)	False Alarm Probability
5155–5272	3660	2.28	0.004	0.064
5520–5623	3744	4.68	0.003	0.099
5899–6018	3171	4.53	0.004	0.000

KELT-19Ab ( $T_{\text{eff}} = 7500$  K,  $\lambda = -179^{\circ}$ ). Thus there are currently too few such systems to draw any conclusions.

The strength of the planet signal in tomography for WASP-180Ab makes it a potential candidate for looking for differential rotation following the RM reloaded technique of Cegla et al. (2016a), through which the effects of differential rotation and the perturbation due to the planet can be disentangled. To bring out the effect of differential rotation on the spectroscopic transit more clearly, the higher spectral resolution and greater light collecting power of ESPRESSO on the VLT would be of use.

## ACKNOWLEDGEMENTS

WASP-South is hosted by the South African Astronomical Observatory and we are grateful for their ongoing support and assistance. Funding for WASP comes from consortium universities and from the UK’s Science and Technology Facilities Council. The research leading to these results has received funding from the European Research Council (ERC) under the FP/2007-2013 ERC grant agreement no. 336480, and under the H2020 ERC grant agreement no. 679030; and from an Actions de Recherche Concertée (ARC) grant, financed by the Wallonia-Brussels Federation. The Euler Swiss telescope is supported by the Swiss National Science Foundation (SNF). TRAPPIST-South is funded by the Belgian Fund for Scientific Research (Fond National de la Recherche Scientifique, FNRS) under the grant FRFC 2.5.594.09.F, with the participation of the SNF. M. Gillon and E. Jehin are F.R.S.-FNRS Senior Research Associates. We acknowledge use of the ESO 3.6-m/HARPS spectrograph under program 0100.C-0847(A), PI C. Hellier. This work has made use of data from the European Space Agency (ESA) mission (<https://www.cosmos.esa.int/gaia>), processed by the *Gaia* Data Processing and Analysis Consortium (DPAC, <https://www.cosmos.esa.int/web/gaia/dpac/consortium>). Funding for the DPAC has been provided by national institutions, in particular the institutions participating in the *Gaia* Multilateral Agreement. This research has also made use of the NASA Exoplanet Archive, which is operated by the California Institute of Technology, under contract with the National Aeronautics and Space Administration under the Exoplanet Exploration Program.

## REFERENCES

- Akeson R. L., et al., 2013, *PASP*, **125**, 989  
 Albrecht S., et al., 2012, *ApJ*, **757**, 18  
 Anderson K. R., Storch N. I., Lai D., 2016, *MNRAS*, **456**, 3671

- Barkaoui K., Gillon M., Benkhaldoun Z., Emmanuel J., Elhalkouj T., Daassou A., Burdanov A., Delrez L., 2017, in *Journal of Physics Conference Series*. p. 012073, doi:10.1088/1742-6596/869/1/012073
- Barkaoui K., et al., 2019, *AJ*, 157, 43
- Blackwell D. E., Shallis M. J., 1977, *MNRAS*, 180, 177
- Brown D. J. A., et al., 2017, *MNRAS*, 464, 810
- Burdanov A., Delrez L., Gillon M., Jehin E., 2018, *SPECULOOS Exoplanet Search and Its Prototype on TRAPPIST*. Springer International Publishing, Cham, pp 1–17, doi:10.1007/978-3-319-30648-3\_130-1, https://doi.org/10.1007/978-3-319-30648-3\_130-1
- Casagrande L., VandenBerg D. A., 2014, *MNRAS*, 444, 392
- Casagrande L., VandenBerg D. A., 2018, *MNRAS*, 475, 5023
- Cegla H. M., Lovis C., Bourrier V., Beeck B., Watson C. A., Pepe F., 2016a, *A&A*, 588, A127
- Cegla H. M., Oshagh M., Watson C. A., Figueira P., Santos N. C., Shelyag S., 2016b, *ApJ*, 819, 67
- Claret A., 2000, *A&A*, 363, 1081
- Claret A., 2004, *A&A*, 428, 1001
- Collier Cameron A., et al., 2007, *MNRAS*, 380, 1230
- Collier Cameron A., Bruce V. A., Miller G. R. M., TriAUD A. H. M. J., Queloz D., 2010, *MNRAS*, 403, 151
- Dai F., Winn J. N., 2017, *AJ*, 153, 205
- Doyle A. P., Davies G. R., Smalley B., Chaplin W. J., Elsworth Y., 2014, *MNRAS*, 444, 3592
- Enoch B., Collier Cameron A., Parley N. R., Hebb L., 2010, *A&A*, 516, A33
- Enoch B., Collier Cameron A., Horne K., 2012, *A&A*, 540, A99
- Gaia Collaboration et al., 2016, *A&A*, 595, A1
- Gaia Collaboration et al., 2018, *A&A*, 616, A1
- Gray R. O., Corbally C. J., 2014, *AJ*, 147, 80
- Green G. M., et al., 2014, *ApJ*, 783, 114
- Green G. M., et al., 2015, *ApJ*, 810, 25
- Gustafsson B., Edvardsson B., Eriksson K., Jørgensen U. G., Nordlund Å., Plez B., 2008, *A&A*, 486, 951
- Hellier C., et al., 2011, in *European Physical Journal Web of Conferences*. p. 01004 (arXiv:1012.2286), doi:10.1051/epjconf/20101101004
- Hirano T., Suto Y., Winn J. N., Taruya A., Narita N., Albrecht S., Sato B., 2011, *ApJ*, 742, 69
- Jehin E., et al., 2011, *The Messenger*, 145, 2
- Marigo P., et al., 2017, *ApJ*, 835, 77
- Mason B. D., Wycoff G. L., Hartkopf W. I., Douglass G. G., Worley C. E., 2001, *AJ*, 122, 3466
- Maxted P. F. L., et al., 2011, *PASP*, 123, 547
- Maxted P. F. L., Serenelli A. M., Southworth J., 2015, *A&A*, 575, A36
- Močnik T., Clark B. J. M., Anderson D. R., Hellier C., Brown D. J. A., 2016, *AJ*, 151, 150
- Neveu-VanMalle M., et al., 2014, *A&A*, 572, A49
- Pepe F., et al., 2002, *The Messenger*, 110, 9
- Petrovich C., 2015, *ApJ*, 799, 27
- Pollacco D. L., et al., 2006, *PASP*, 118, 1407
- Pollacco D., et al., 2008, *MNRAS*, 385, 1576
- Pont F., Husnoo N., Mazeh T., Fabrycky D., 2011, *MNRAS*, 414, 1278
- Queloz D., et al., 2001, *The Messenger*, 105, 1
- Sestovic M., Demory B.-O., Queloz D., 2018, *A&A*, 616, A76
- Sivard R. J., et al., 2018, *AJ*, 155, 35
- Stassun K. G., Torres G., 2018, *ApJ*, 862, 61
- Storch N. I., Lai D., Anderson K. R., 2017, *MNRAS*, 465, 3927
- Temple L. Y., et al., 2017, *MNRAS*, 471, 2743
- Temple L. Y., et al., 2018a, preprint, (arXiv:1811.05742)
- Temple L. Y., et al., 2018b, *MNRAS*, 480, 5307
- Torres G., Andersen J., Giménez A., 2010, *A&ARv*, 18, 67
- TriAUD A. H. M. J., 2017, *The Rossiter–McLaughlin Effect in Exoplanet Research*. Springer International Publishing, Cham, pp 1–27, doi:10.1007/978-3-319-30648-3\_2-1, https://doi.org/10.1007/978-3-319-30648-3\_2-1
- Weiss A., Schlattl H., 2008, *Ap&SS*, 316, 99
- Winn J. N., Fabrycky D., Albrecht S., Johnson J. A., 2010, *ApJ*, 718, L145

This paper has been typeset from a T<sub>E</sub>X/L<sup>A</sup>T<sub>E</sub>X file prepared by the author.